Left Ventricular Segmentation of Cardiac Magnetic Resonance Images Using a Novel Edge Following Technique

Krit Somkantha and Nipon Theera-Umpon
Department of Electrical Engineering
Faculty of Engineering, Chiang Mai University,
Biomedical Engineering Center, Chiang Mai University,
Chiang Mai 50200 Thailand
nipon@ieee.org

Sansanee Auephanwiriyakul
Department of Computer Engineering
Faculty of Engineering, Chiang Mai University,
Biomedical Engineering Center, Chiang Mai University,
Chiang Mai 50200 Thailand

Abstract—This paper presents a novel edge following technique for image segmentation designed to segment the left ventricle in cardiac magnetic resonance (MR) images. This is a required step to determine the volume of left ventricle in a cardiac MR image, which is an essential tool for cardiac diagnosis. The traditional method for extracting them from cardiac MR images is by human delineation. This method is accuracy but time consuming. So a new ventricular segmentation technique is proposed in order to reduce the analysis time with similar accuracy level compared to doctors' opinions. Our proposed technique can detect ventricle edges in MR images using the information from the vector image model and the edge map. We also compare the proposed segmentation technique with the active contour model (ACM) and the gradient vector flow (GVF) by using the opinions of two skilled doctors as the ground truth. The experimental results show that our technique is able to provide more accurate segmentation results than the classical contour models and visually close to the manual segmentation by the experts. The results evaluated using a numerical measure by mean of the probability of error in image segmentation also confirm the visual evaluation.

Keywords—magnetic resonance images, left ventricular segmentation, vector field model, active contour model, gradient vector flow model

I. INTRODUCTION

Magnetic resonance imaging (MRI) is a non-invasive tool that can be used to measure the deformation of hearts and to diagnose the presence of heart diseases by analyzing the heart function throughout the cardiac cycle [1],[2]. Left ventricular segmentation of a cardiac magnetic resonance (MR) image is challenging due to poor image contrast and high noises. Finding the correct segmentation of a cardiac MR image is a difficult task. The accurate detection of boundaries from the MR images plays a key role in many applications and essential to many diagnostic and treatment procedures such as the congestive heart failure and the cardiac hypertrophy. Usually doctors have to draw contours manually, slice by slice, in order to calculate volume information of the left ventricle. This is a tedious work and delays the whole diagnosis procedures. So

reducing the variability and time constraints inherent in manual segmentation is an essential tool for cardiac diagnosis.

Many automated segmentation algorithms have been developed. However, to delineate the structures of interest and discriminate them from the background automatically poses considerable challenges. All conventional edge detection techniques, e.g., Roberts, Sobel, Prewitt, Laplacian, and Canny, are all based on the difference of gray levels [3]-[8]. However, they fail to extract the correct boundaries in MR images. Several methods have also been developed to process the acquired images and identify features of interest such as intensity-based method and region-growing methods [9]. Intensity-based methods identify local features such as edges and texture in order to extract regions of interest. Region-growing methods start from a seed-point (usually chosen by a user) on image and perform the segmentation task by clustering neighborhood pixels using a similarity criterion.

Active contour models (ACM) also known as snakes are curves defined within an image domain that can be moved under the influence of internal energy and external energy [10]-[12]. The internal energy is designed to keep the model smooth during deformation. The external energy is defined to move the model toward an object boundary or other desired features within an image. The snake has weakness and limitations of small capture range and difficulties progressing into concave boundary regions. The gradient vector flow (GVF) or the GVF-snake is an active contour model with a new external energy [13],[14]. This new external energy was computed as a diffusion of gray-level gradient vector of a binary edge map derived from the image. The resultant field has a large capture range and forces active contours into concave regions. The snake model has attracted many researchers attention due to the good performance [15]-[17]. However, most snake models for finding the optimal edges have difficulties in medical images in which ill-defined edges are encountered.

To remedy the problem, we propose a method for segmenting ventricle boundaries in cardiac MR images using a novel edge following. The proposed edge following technique is based on the vector image model and the edge map. The

vector image model provides a more complete description of an image in which both directions and magnitudes of image edges are considered. From the vector image model, a derivative-based edge operator is applied to yield the edge vector field [18],[19]. The proposed edge vector field is generated by averaging magnitudes and directions in the vector image. The edge map is derived from the Law's texture features [20],[21] and the Canny edge detection. The vector image model and the edge map are used to select the best edges.

II. AVERAGE EDGE VECTOR FIELD MODEL

We exploit the edge vector field to devise a new boundary extraction algorithm. The edge vector field is calculated according to the following equations [18],[19]:

$$\vec{e}(i,j) = \frac{1}{k}\left(M_x(i,j)\vec{i} + M_y(i,j)\vec{j}\right), \qquad (1)$$

$$\vec{e}(i,j) \approx \frac{1}{k}\left(\frac{\partial f(x,y)}{\partial y}\vec{i} - \frac{\partial f(x,y)}{\partial x}\vec{j}\right), \qquad (2)$$

where

$$k = \max_{i,j}\left(\sqrt{M_x(i,j)^2 + M_y(i,j)^2}\right). \qquad (3)$$

Each component is the convolution between the image and the corresponding difference mask, i.e.,

$$M_x(i,j) = -G_y * f(x,y) \approx \frac{\partial f(x,y)}{\partial y}, \qquad (4)$$

$$M_y(i,j) = G_x * f(x,y) \approx -\frac{\partial f(x,y)}{\partial x}, \qquad (5)$$

where $f(x,y)$ is an input image, G_x and G_y are the difference masks of the Gaussian weighted image moment vector operator, i.e.,

$$G_x(x,y) = \frac{1}{\sqrt{2\pi}\sigma}\left(\frac{x}{\sqrt{x^2+y^2}}\right)\exp\left\{\left(-\frac{x^2+y^2}{2\sigma^2}\right)\right\}, \quad (6)$$

$$G_y(x,y) = \frac{1}{\sqrt{2\pi}\sigma}\left(-\frac{x^2+y^2}{2\sigma^2}\right)\exp\left\{\left(\frac{y}{\sqrt{x^2+y^2}}\right)\right\}. \quad (7)$$

Edge vectors of an image indicate the magnitudes and directions of edges that form a vector stream flowing around an object. In an unclear image, the vectors may distribute randomly in magnitude and direction. Therefore we extend the capability of the previous edge vector field by applying a local averaging operation where the value of each vector is replaced by the average of all the values in the local neighborhood.

$$M(i,j) = \frac{1}{M_r}\sum_{(i,j)\in N}\sqrt{M_x(i,j)^2 + M_y(i,j)^2} \qquad (8)$$

$$D(i,j) = \frac{1}{M_r}\sum_{(i,j)\in N}\tan^{-1}\left(\frac{M_y(i,j)}{M_x(i,j)}\right) \qquad (9)$$

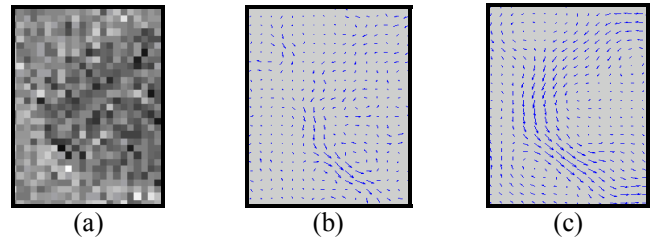where M_r is the total number of pixels in the neighborhood N.

Figure 1. Vector fields of unclear images (a) Original image (b) Result from edge vector field (c) Result from the proposed average edge vector field.

An example of the derived edge vector field calculated by averaging both of direction and magnitude is shown in figure 1(c). Figures 1(b) and 1(c) show that our proposed edge vector field yields more descriptive vectors along the object edge than that of the original edge vector field.

III. EDGE MAP

Edge map is edges of an image derived from Law's texture features and the Canny edge detection. It gives information of image which is exploited in a decision for edge following.

A. Law's Texture

The texture feature images are computed by convolving an input image with each of the masks. The 2-dimensional convolution masks typically used for texture discrimination are generated from the following set of 1-dimensional convolution masks of length five:

- local averaging filter   L5=(1,4,6,4,1)

- edge detector   E5=(−1,−2,0,2,1)

- spot detector   S5=(−1,0,2,0,−1)

- ripple detector   R5=(1,−4,6,−4,1)

- wave detector   W5 =(−1,2,0,−2,1)

If we multiply the column vectors and row vectors of the masks shown above, we obtain 25 Law's masks. We can obtain the output image $t(i,j)$ by convolving the input image with texture masks, i.e.,

$$t(i,j) = l(i,j) * f(i,j), \qquad (10)$$

$$t(i,j) = \sum_{m=-2}^{m=2}\sum_{n=-2}^{n=2} l(m,n)f(i+m,j+n), \qquad (11)$$

where $l(i, j)$ is the 2-D masks from Law's texture and $f(i, j)$ is the input image.

B. Canny Edge Detection

The Canny approach to edge detection is optimal for step edges corrupted by white Gaussian noise. This edge detector is assumed to be the output of a filter that both reduces the noise and locates the edges. It is well described in the literature. Therefore, we briefly describe it here. The first step of Canny edge detection is to convolve the texture image with a Gaussian filter. The second step is to calculate the magnitude and direction of the gradient. The third step is nonmaximal suppression (nms) to identify edges. The broad ridges in the magnitude must be thinned so that only the magnitudes at the points of greatest local change remain. The last step is the double thresholding algorithm to detect and link edges.

We try to apply the Canny edge detection to left ventricular in cardiac magnetic resonance images. An example of the edge map derived from the Law's texture L5L5 and the Canny edge detection is shown in figure 2.
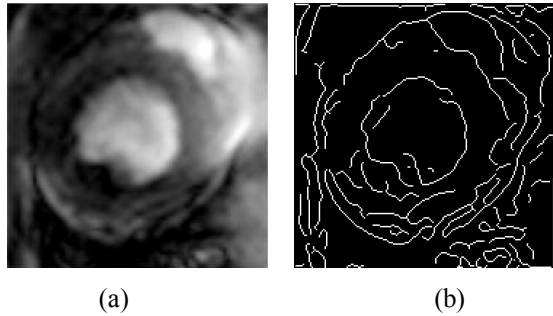

(a)   (b)

Figure 2.   (a) Original image (b) Result from edge map which derived from Law's texture(L5L5) and Canny edge detection.

IV.   PROPOSED EDGE FOLLOWING TECHNIQUE

The proposed edge following technique is based on the aforementioned vector image model and edge map. At the position (i, j) of an image, the 3×3 matrices $\mathbf{M}_{ij}$, $\mathbf{D}_{ij}$, and $\mathbf{E}_{ij}$ are calculated as follows:

$$\mathbf{M}_{ij}(r,c) = \frac{M(i+r-1, j+c-1)}{\max M(i,j)}, \quad 0 \le r,c \le 2 \quad (12)$$

$$\mathbf{D}_{ij}(r,c) = 1 - |D(i,j) - D(i+r-1, j+c-1)|, \quad 0 \le r,c \le 2 \quad (13)$$

$$\mathbf{E}_{ij}(r,c) = E(i+r-1, j+c-1), \quad 0 \le r,c \le 2 \quad (14)$$

where $M(i, j)$ and $D(i, j)$ are the proposed average magnitude and direction of the edge vector field as shown in Eq. (8) and (9), respectively. $E(i, j)$ is the edge map from the Law's texture and Canny edge detection. It should be noted that the values of each element in the matrices $\mathbf{M}_{ij}$, $\mathbf{D}_{ij}$, and $\mathbf{E}_{ij}$ are ranged between 0 and 1.

Another auxiliary matrix $\mathbf{L}_{ij}$ corresponding to the position (i, j) is defined as

$$\mathbf{L}_{ij} = \alpha\mathbf{M}_{ij} + \beta\mathbf{D}_{ij} + \varepsilon\mathbf{E}_{ij}, \quad (15)$$

where α, β, and ε are the weight parameters that control the edge to flowing around an object. The larger value of an element in $\mathbf{L}_{ij}$ indicates the stronger edge in the corresponding direction. The total value of all weight parameters are set to 1. In our experiments we set $\alpha = 0.6$, $\beta = 0.2$, and $\varepsilon = 0.2$.

At the position (i, j), the most likely direction linked to the next edge pixel can be calculated by

$$D_{ij,opt} = \arg\max_k \sum_{r=0}^{2}\sum_{c=0}^{2} \mathbf{L}_{ij}(r,c)\mathbf{C}_k(r,c), \quad (16)$$

where $k = 1, 2, \ldots, 8$, denotes the 8 directions as indicated by the arrows at the center of each mask shown in figure 3. The 3×3 masks $\mathbf{C}_k$ are also shown in figure 3. The values of each element in each mask dictate the corresponding direction. The edge following is continued until there is no change in the list of edge pixels.
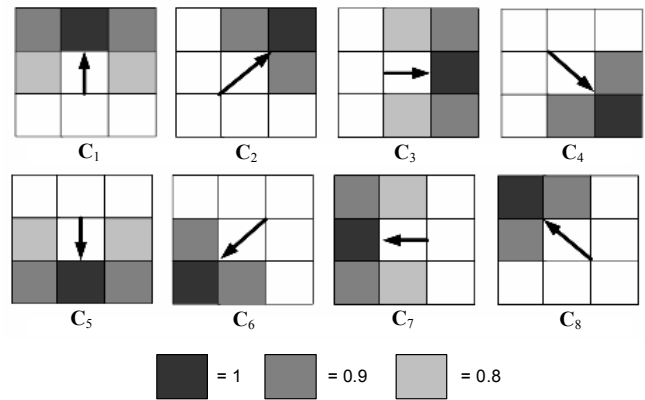

Figure 3.   The normal direction constraint.

V.   EXPERIMENTAL RESULTS

We apply the proposed edge detection algorithm to segment the left ventricles in cardiac magnetic resonance images. The comparisons of the result of the proposed technique with two conventional edge detection methods, i.e., the active contour model (ACM) and the gradient vector flow (GVF)-snake are shown in figure 4. To make the comparison fair to all methods, their initial contours (snakes) are selected manually as shown in figure 4(a). We can see that the results from our proposed method are visually better than that from the ACM and the GVF-snake.
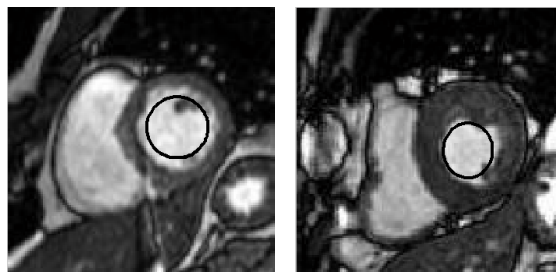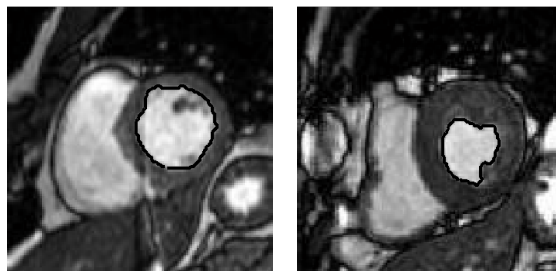
(a)
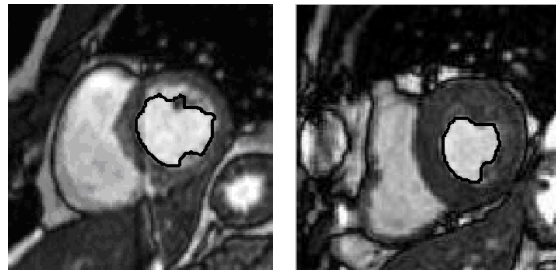
(b)
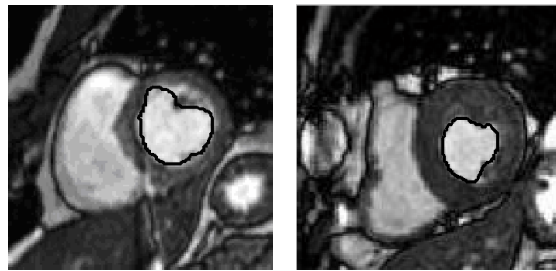
(c)

(d)

Figure 4.   (a) Original image and initial circle (b)-(c) Results from ACM and GVF-snake with $\alpha = 0.05, \beta = 0, \gamma = 1, \sigma = 1$, (d) Results from the proposed technique.

To further evaluate the efficiency of the proposed segmentation method, we compare the contours obtained using the ACM, the GVF-snake, and the proposed method with those manually drawn by a skilled doctor. Figure 5 shows the segmentation results on other two cardiac MR images. Again, our proposed method yields the contours that are very close to the expert's opinions.
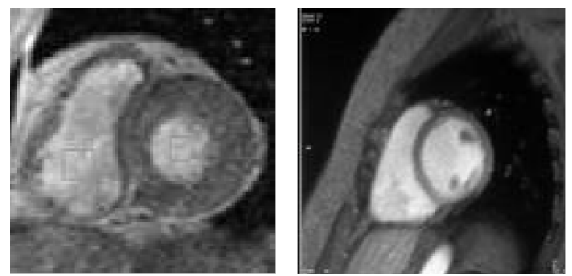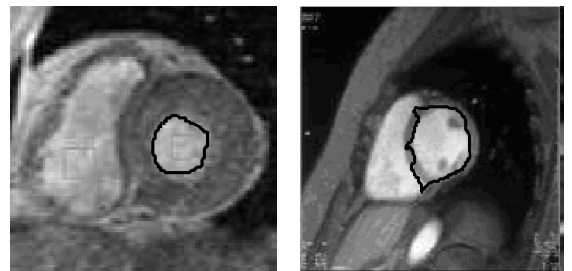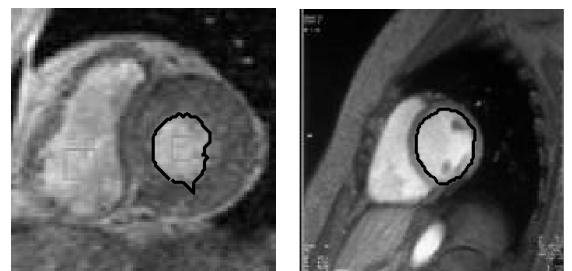

(a)
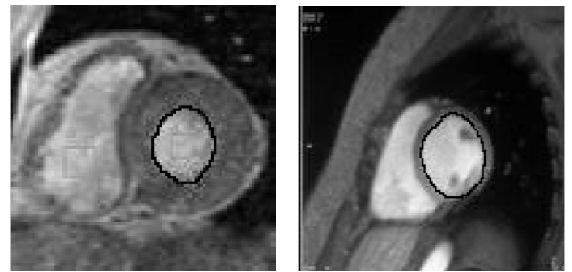
(b)
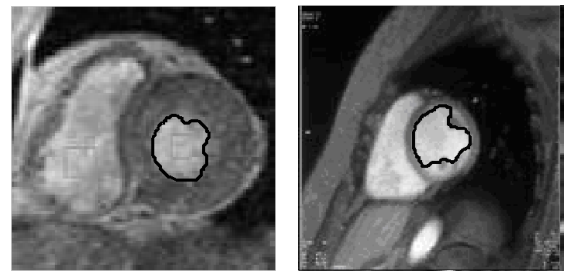
(c)

(d)

(e)

Figure 5.   (a) Original image (b) Doctor's delineation (c)-(d) Results from ACM and GVF-snake (e) Results from the proposed technique.

In addition to the visual inspection, we evaluate our segmentation method numerically using the probability of error in image segmentation

$$PE = P(O)P(B \mid O) + P(B)P(O \mid B), \qquad (17)$$

where $P(O)$ and $P(B)$ are *a priori* probabilities of objects and background in images. $P(B \mid O)$ is the probability of error in classifying objects as background. $P(O \mid B)$ is the probability of error in classifying background as objects [22]-[25].

To also investigate the variation among doctors' opinions on this problem, we ask another skilled doctor to delineate contours of ventricles in the MR images. The PEs on the segmentation by both doctors are depicted in Table I. They show that the experts can even have the disagreement by about 13.6% on average. The PEs on the results from the proposed method, the ACM, and the GVF-snake compared to the two doctor's opinions on 10 MR images are shown in Table II.

TABLE I.   PROBABILITY OF ERROR IN IMAGE SEGMENTATION (PE) BETWEEN TWO SKILLED DOCTORS.

MR Image	PE of Doctor1 and Doctor2
1	4.80%
2	5.80%
3	21.41%
4	14.44%
5	7.81%
6	22.78%
7	7.50%
8	20.14%
9	20.91%
10	10.79%
Average	13.63%

TABLE II.   RESULTS ON MR IMAGE BY MEAN OF PROBABILITY OF ERROR IN IMAGE SEGMENTATION (PE).

MR Image	Proposed Method		ACM		GVF-Snake	
	Doctor1	Doctor2	Doctor1	Doctor2	Doctor1	Doctor2
1	4.84%	6.27%	27.47%	28.54%	23.99%	25.04%
2	5.80%	7.28%	43.95%	34.71%	15.07%	15.17%
3	12..34%	16.85%	28.69%	24.32%	22.63%	29.45%
4	12..93%	7.92%	21..32%	15.03%	30.07%	32.44%
5	10.79%	11.63%	22.83%	21.32%	53.61%	44.32%
6	10.71%	15.44%	9.55%	15.85%	30.74%	28.86%
7	8.79%	10.00%	12.33%	14.00%	10.19%	10.00%
8	9.33%	16.77%	40.44%	30.95%	14.93%	14.78%
9	11.13%	16.80%	31.44%	23.07%	14.71%	14.11%
10	11.34%	6.43%	10.62%	6.44%	12.07%	7.66%
Average	7.27%	11.53%	22.73%	21.42%	22.80%	22.18%

We see that the proposed method yields segmentation results much closer to both experts' opinions than that of the ACM and the GVF-snake. Moreover, the disagreement between the proposed method and each of the doctors is less than the disagreement among both doctors themselves.

VI.   CONCLUSION

In this paper, we propose a novel edge following technique and apply it to segment the left ventricle in cardiac magnetic resonance images. The proposed edge following technique incorporates a vector image model and the edge map information. Segmentation results from our proposed method are compared with doctors' delineation. We also compare the proposed method with two popular methods for detecting ill-defined edges, i.e., the active contour model and the gradient vector flow, using the doctors' opinion as the ground truth. The experimental results show that the proposed method yields very effective edge detection performances and is better than the conventional counterparts on this particular problem. The proposed method can further be applied to any image processing problems in which the ill-defined edge detection is encountered.

REFERENCES

[1]   R.J. van Der Geest and J.H. Reiber, "Quantification in cardiac MRI," J.Magn. Reson. Imag., vol. 10, pp. 602-608, 1999.

[2]   R.I. Pettigrew, J.N. Oshinski, G.Chatzimavroudis, and W.T. Dixon, "MRI techniques for cardiovascular imaging," J. Magn. Reson. Imag., vol. 10, pp. 590-601, 1999.

[3]   J.R. Parker, Algorithms for Image Processing and Computer Vision, Wiley Computer Publishing, 1997.

[4]   R.C. Gonzalez and R.E. Woods, Digital Image Processing. Reading, MA: Addison Wesley, reprint, 1992.

[5]   J. M. S. Prewitt, "Object enhancement and extraction," Picture Processing and Psychopictorics," Proc. IEEE, vol. 59, pp.75-149, 1970.

[6]   G.S. Robinson, "Edge detection by compass gradient masks," Compute. Graph. Image Processing., vol.6,pp. 492-501, 1977.

[7]   E. Argyle, "Techniques for edge detection," Proc. IEEE,, pp. 285-287, 1970.

[8]   J. F. Canny, "A computational approach to edge detection," IEEE Trans. Pattern Anal. Machine Intell., vol. PAMI-8, pp. .679-698, 1986.

[9]   P.J. Besl and R.C. Jane, "Segmentation through variable-order surface fitting," IEEE Trans. Pattern Anal. and Machine Intell., vol. 10(2), pp. 167-192, 1988.

[10]   V. Caselles, F. Catte, T. Coll, and F. Dibos. "A geometric model for active contours," Numer Math, vol. 66, pp.1–31. 1993.

[11]   F. Leymarie and M.D. Levine, "Tracking deformable objects in the plane using an active contour model," IEEE Trans. Pattern Anal. and Machine intell., vol. 15, pp. 617-634, 1993.

[12]   M. Kass, A. Witkin, and D. terzopoulos. "Snakes: active contour models," International Journal of Computer vision, vol 1:pp.321-331, 1987.

[13]   C. Xu, and J.L. Prince, "Gradient vector flow: A new external force for snake," IEEE Proc. Conf. on Comp. Vis. Patt Recog., pp. 66-71, 1977.

[14]   C. Xu, and J.L. Prince, "Snakes, shapes, and gradient vector flow," IEEE Trans. on Image Processing, vol. 7(3), pp. 359-369, 1998.

[15]   A. Caro, P.G. Rodriguez, E. Cernadas, M.L. Duran and   T. Antequera, "Potential field as and external force and algorithmic improvements in deformable models," Electronic Letters on Computer vision and Image Analysis, vol. 2(1), pp. 25-36, 2003.

[16]   C. Sagiv, N.A. Sochen, and Y.Y. Zeevi, "Integrated active contours for texture segmentation," IEEE Trans. Image Processing, vol. 15(6), pp. 1633-1646, 2006.

[17]   J. Cheng and S.W. Foo, "Dynamic directional gradient vector flow for snakes", IEEE Trans. Image Processing, vol. 15(6), pp. 1563-1571, 2006.

[18]   N. Eua-Anant and L. Udpa, "A novel boundary extraction algorithm based on a vector image model," Proc. IEEE, pp.597-600, 1997.

[19] N. Eua-Anant and L. Udpa, "Boundary detection using simulation of particle motion in a vector image field," IEEE Trans. Image Processing, vol 8(11), pp. 1560-1571, 1999.

[20] K. Laws, Textured Image Segmentation, Ph.D. Dissertation, 1980.

[21] K. Laws, "Rapid texture identification," SPIE, vol. 238, pp. 376-380, 1980.

[22] N. Theera-Umpon, "Patch-based white blood cell nucleus segmentation using fuzzy clustering," ECTI Trans. Elec. Eng., Electron., and Comm., vol. 3(1), pp. 15-19, 2005.

[23] N. Theera-Umpon, "White blood cell segmentation and classification in microscopic bone marrow images", Lecture Notes in Computer Science, vol. 3614, pp. 787-792, 2005.

[24] S.U. Lee, S.Y. Chung, R.H. Park, "A comparative performance study of several global thresholding techniques for segmentation," Computer Vision, Graphics, and Image Processing, vol. 52(2), pp. 171–190, 1990.

[25] X.W. Zhang, J.Q. Song, M.R. Lyu, S.J. Cai, "Extraction of karyocytes and their components from microscopic bone marrow images based on regional color features," Pattern Recognition, vol. 37(2), pp. 351–361, 2004.